

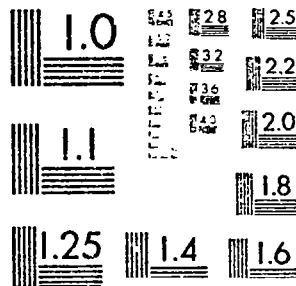


0062714

1 OF 1

N76 26425

UNCLAS



MICROCOPY  
NATIONAL B

LOAN COPY: RETURN TO  
AFWL TECHNICAL LIBRARY  
KIRTLAND AFB, N.M. 87117



0062714

AN EXPERIMENTAL INVESTIGATION OF AN AXISYMMETRIC  
JET IN A COFLOWING AIRSTREAM<sup>+</sup>

by

G. D. Catalano  
J. B. Morton  
R. R. Humphris

(NASA-CR-143104) AN EXPERIMENTAL  
INVESTIGATION OF AN AXISYMMETRIC JET IN A  
COFLOWING AIRSTREAM (Virginia Univ.) 37 p  
HC \$4.00 CSCI 20D

N76-26425

G3/34 Unclass  
43049

Department of Engineering Science and Systems  
RESEARCH LABORATORIES FOR THE ENGINEERING SCIENCES  
SCHOOL OF ENGINEERING AND APPLIED SCIENCE  
UNIVERSITY OF VIRGINIA  
CHARLOTTESVILLE, VIRGINIA

Report No. ESS-4043-106-75

July 1975, Revised February 1976

<sup>+</sup> This work was supported in part by NASA Grant No. NGR 47-005-219 and  
by NSF Grant No. GK-40126.

# ABSTRACT

An experimental investigation of the flow development of an axisymmetric jet exhausting into a moving airstream has been made. The jet has a Reynolds number of 22,600 and the ratio of the jet velocity to the wind tunnel velocity ( $\lambda_j$ ) is 5.1 to 1. The flow field of the axisymmetric jet was examined at locations varying from approximately zero to eight diameters downstream of the orifice. Of primary concern at each downstream location was the mapping of the one point statistical properties of the flow, including mean velocity, turbulent intensity, and intermittency. Autocorrelations and power spectral density curves were determined for both the fluctuating velocity field and the concentration signal at various distances from the jet's center line for different downstream locations. A laser-Doppler velocimeter, using a phase locked-loop processor, was used to make the desired velocity field measurements which were compared with hot wire anemometer and pressure probe data. To determine the intermittency profiles, velocity-concentration correlations and concentration power spectra, a laser light scattering technique was employed.

# LIST OF SYMBOLS

$b(x)$	Radial Distance between .20 U max location and .80 U max location
$D$	Diameter of nozzle
$e$	Base of natural logarithms
$f$	Frequency of fluctuations
$F$	Spectral density
$f_D$	Doppler shift in frequency
$f_P$	Frequency at which peak in spectrum appears
$I$	Intermittency
$k_r$	Wave vector for incident light
$k_s$	Wave vector of scattered light
$L$	Longitudinal integral scale
$P$	Velocity of smoke particle
$r$	Radial distance from centerline of flow
$r_m$	Half width of jet
$r_o$	Radius of nozzle
$R$	Autocorrelation coefficient
$Re$	Reynolds number
$R_{uu'}$	Two point correlation coefficient
$R_{u\theta}$	Velocity-concentration correlation coefficient
$S_{tr}$	Strouhal number
$t$	Time
$\Delta t$	Increment in time
$u, u'$	Velocity fluctuations in longitudinal direction

# LIST OF SYMBOLS (continued)

$U$	Mean velocity at LDV probe position
$U_{FS}$	Free stream velocity
$U_{max}$	Mean velocity at centerline at each downstream location
$U_o$	Maximum mean velocity of jet at exit plane
$v$	Velocity fluctuations in radial direction
$V$	Mean velocity in radial direction
$x$	Downstream distance from exit plane of jet
$\beta$	Scattering angle
$\theta$	Instantaneous concentration fluctuation
$\lambda_j$	Ratio of jet exit plane velocity to free stream velocity
$\lambda_o$	Wavelength of monochromatic laser beam
$\lambda_T$	Taylor microscale
$\overline{(\quad)}$	The mean value of the quantity

## INTRODUCTION

With the increasing need for mass urban rapid transit systems, aerospace designers have looked to improve the present STOL and V/STOL capabilities in order that aircraft can be flown into and from places which do not have large areas available for long and costly runways. Several jet/aerofoil configurations have been proposed which may prove feasible in increasing the short take-off and landing capabilities of aircraft. One of the designs currently under investigation is called upper surface blowing. In this configuration, jet engines are mounted on the upper surface of the wing. The jet exhaust is then turned by the presence of the wing surface and added lift results. However, the buffeting that the wing and any trailing flaps must endure is quite severe. Thus the need exists for a more thorough investigation of the "near field" of the jet and how the wing surface affects the jet exhaust.

This investigation deals with the problem of an axisymmetric jet exhausting into a slower moving secondary stream. Presently, the concern is solely in determining the one point statistical properties in the resultant flow field. Once this is done, aerofoil type structures can be positioned in the flow to determine their effects on the one point statistical properties of the jet. This will be the subject of a later paper. The secondary stream outside the actual jet flow presents the opportunity to simulate dynamic as well as static conditions for testing various jet/aerofoil configurations.

The main physical features of a subsonic jet are described by Davies.<sup>(1)</sup> At the jet orifice, there exists a thin, cylindrical vortex sheet which rapidly develops into a layer of highly sheared strong turbulence. This settles down to an annulus of strongly sheared, kinematically similar, intense turbulence surrounding a core of potential flow after approximately 1 diameter. The statistical and geometric characteristics of the flow remain similar for another 4 or 5 diameters. A second adjustment region follows where the potential core has vanished and the mean shear decreases rapidly.<sup>(2)</sup>

This report is based on the master's thesis of George D. Catalano, University of Virginia, Charlottesville, Virginia, May, 1975.

Experimental data on the near field problem has increased markedly in the past few years. Lau and Fisher<sup>(3)</sup> found that the suggestion of a vortex street for modelling the structure of a round turbulent jet is well founded. Sami, Carmody and Rouse<sup>(4)</sup> through use of measured distributions of mean flow and turbulence characteristics evaluated all terms of the integral and differential forms of the momentum and mean energy equations. Sami<sup>(5)</sup> concluded the investigation by studying the turbulence energy equation and in addition investigated axial, radial and tangential scales of turbulence.

In the mixing region of a free jet, Davies found that the statistical properties of the turbulence can be expressed in terms of kinematic similarity relationships based on the jet diameter and axial distance as length scales and the inverse local shear as a time scale. The turbulent mixing of two jets of fluid of the same density was investigated theoretically by means of Prandtl's theory of turbulence and the results compared with experiment by Kuethe.<sup>(6)</sup> Momentum and mass transfer in coaxial gas jets were considered by Forstall and Shapiro.<sup>(7)</sup> They concluded that material diffuses more rapidly than momentum which was in agreement with Alpinieri<sup>(8)</sup> and that the principal independent variable determining the shape of the mixing region is the velocity ratio of the streams. For a two dimensional incompressible mixing layer, Wygnanski and Fiedler<sup>(9)</sup> found that the mixing region can be divided into two regions, one on the high velocity side which resembles the outer part of a wake and the other on the low velocity side which resembles a jet.

Antonia and Bilger<sup>(10)</sup> in their investigation of an axisymmetric jet in a coflowing stream found that the turbulence structure of the flow indicates that self-preservation does not apply for this situation and that the flow far downstream depends strongly on the complete past history. Finally, Corrsin and co-investigators have made the most complete measurements including the temperature as well as the velocity field of a heated jet.<sup>(11-13)</sup> Szablewski looked at the diffusion of a hot air jet in a coflowing stream.<sup>(14)</sup>

## INSTRUMENTATION AND TEST FACILITIES

While the principle of Doppler frequency shift of electromagnetic waves due to scattering by moving bodies has been known for some time, the first practical arrangements of laser-Doppler velocimetry were introduced in 1964.<sup>(15)</sup> In recent years, the laser-Doppler velocimeter has been rapidly developed to measure flow velocities in laminar and turbulent flows.<sup>(16-18)</sup>

If  $k_r$  and  $k_s$  are wave vectors of the incident and scattered radiation, and  $P$  is the velocity component in the  $(k_s - k_r)$  direction then the frequency shift  $f_D$  is

$$f_D = (2P/\lambda_0) \sin (\beta/2)$$

where  $\beta$  is the angle between the two beams and  $\lambda_0$  is the wavelength of monochromatic laser beam.

To measure the concentration field of the turbulent jet, a laser light scattering technique based on the one developed by Rosenweig<sup>(19)</sup> was employed. The system used here was developed and studied in detail by Shaughnessy.<sup>(20)</sup>

### OPTICAL SYSTEMS

An argon ion laser was used as the light source for both the velocity and the intermittency measurements. For a single wavelength operation at 514.5 nm, the maximum power output was 1 watt with a noise level of less than 1%. The beam's diameter at the  $\frac{1}{e^2}$  points was 1.5 mm at the laser head and approximately 2 mm in the test section.

To determine the velocity field quantities of the flow, the reference beam mode of operation was employed. The optical system consisted of a



beam splitter and mirror which produce two parallel beams of light, and a lens with a focal length of 30 cm. A #2 neutral density filter was placed in the reference beam's path. The control volume for this set up was found to be 0.05 mm (diameter)  $\times$  1 mm (height).<sup>(21)</sup> The entire optical assembly was mounted on an aluminum slide which provides movement of the control volume in a horizontal direction perpendicular to the jet and tunnel flow axes. The detection system consisted of a photodiode with its associated electronics. The diode had an active surface diameter of 2.7 mm.

To determine the intermittency profiles, the optical system developed by Shaughnessy<sup>(20)</sup> was utilized. The design included a lens mirror assembly which permitted the selection of virtually any size control volume from .1 mm by .1 mm by .1 mm to 1.5 mm  $\times$  1.5 mm  $\times$  1.5 mm. The detection system used a PIN silicon photodiode with an active surface diameter of .51 mm mounted behind a spatial filter. The spatial filter assembly was composed of a simple lens and an aperture located in the focal plane of the image formed. The lens of the spatial filter assembly was positioned for unit magnification. The effects of ambiguity noise, optical path noise and other sources of noise on the performance of the laser-light scattering system were discussed by Shaughnessy.<sup>(20)</sup>

#### SIGNAL PROCESSING

In this investigation, the jet was marked with dioctyl phthalate (DOP) smoke while the tunnel flow was kept clean. Since the Schmidt number was very high ( $\sim 10^4$ ), the smoke remained confined to the jet. The only way clean air could be marked by the DOP was by being entrained into the jet. Thus, outside the potential core region, the presence of smoke indicated the presence of turbulence.

When the measurement point was located in a highly intermittent region (sometimes inside the jet - sometimes not), the signal processor received a highly intermittent signal. This signal was characterized by periods of "dead time" (i.e., no smoke particles present) interspersed with Doppler frequency bursts. To test the response of the electronic signal processor to a flow of this nature, an experiment was devised which would determine the accuracy of the statistical properties measured by the phase

locked-loop system. The experiment (c.f. Figure 1) consisted of initially locating the control volume in an area of the flow field where smoke particles were present 100% of the time. The mean velocity and the mean square of the velocity fluctuations were recorded. Next, a rotating disk was inserted in the path of the beam. Increasing amounts of the disk were removed (12.5%, 25% and 50% ) to simulate intermittencies of 12.5%, 25%, and 50%. The mean velocity and mean square of the velocity fluctuations,  $\overline{u^2}$ , are noted in Table 1. The results indicate that the mean velocity is essentially independent of the value of intermittency at the control volume's position. Also the mean square of the velocity fluctuation is directly proportional to the value of the intermittency.

It should be noted that only velocities inside the jet were measured by this system. Thus the measurements should be considered as "conditionally sampled."

Table 1

<u>Intermittency</u>	<u>Mean Velocity</u>	<u>Turbulent Intensity</u>	<u>Turbulent Intensity/ Intermittency</u>
(I)	(U)	$\frac{\overline{u^2}}{\overline{U^2}}$	$\frac{\overline{u^2}}{\overline{U^2} \times I}$
100%	9.13m/sec	9.75%	9.75%
50%	9.11m/sec	4.83%	9.66%
25%	9.11m/sec	2.44%	9.75%
12.5%	9.11m/sec	1.22%	9.82%

#### THE FLOW SYSTEM

A jet whose compressed air is marked with dioctyl phthalate (DOP) was mounted inside the test section of a low turbulence level subsonic wind tunnel (Figure 2). With the parallel secondary flow in the wind tunnel kept at a constant speed of 3.20m/sec, the ratio of the exit plane velocity of the jet to the velocity of the tunnel, ( $\lambda_j$ ), was 5.1 : 1. The jet with a contraction ratio of 14 to 1 over a length of 15.9 cm. had a Reynolds number of 22,600 and an exit plane diameter of 2.14 cm.

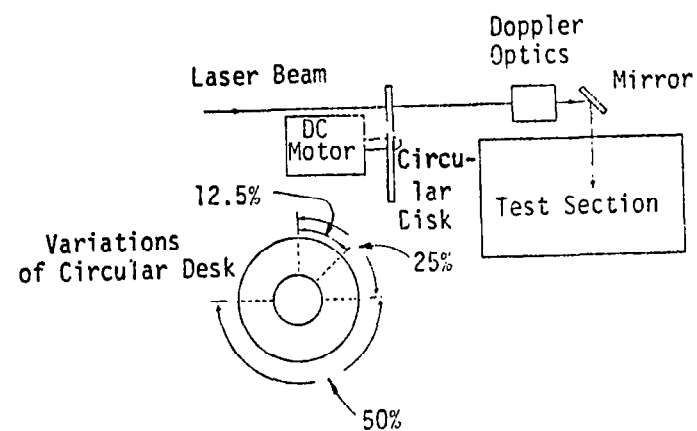


Figure 1 Variable Intermittency Checkout of the Phase Locked-Loop Device

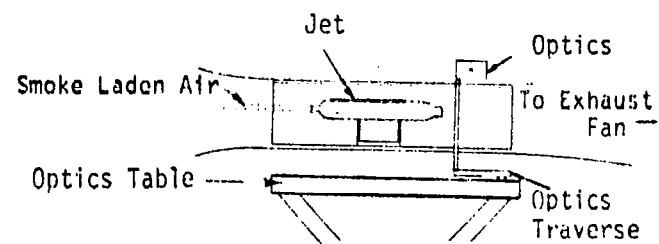


Figure 2 Schematic of Laboratory Facility

Since the experimental design upstream of the jet exit was an important parameter, several methods were used in determining the actual conditions. First, smoke (DOP) was injected into the outer wind tunnel flow field and the region near the contraction section of the jet itself was closely monitored. No evidence of separation of the outer flow from the jet was observed. Secondly, pitot-static tube profiles were taken for several  $x/D$  locations. Two such profiles are shown in Figure 3. At  $x/D = 0$ , the mean velocity was zero at the lip of the jet and then reached the free stream value at approximately 3 radii from the lip. At  $x/D = 1$ , the velocity defect had decreased so that the smallest fluid velocity is about half the value of the free stream velocity. This trend continued until at  $x/D = 6$ , virtually no defect at all was apparent.

Finally, a pressure probe connected to a 1/8 inch condenser type microphone was traversed along the outside of the contraction section of the jet. By the sound produced, it was easy to distinguish between laminar and turbulent flow. Once again, no evidence of separation of tunnel flow from the jet assembly was found.

#### EXPERIMENTAL RESULTS

In this section, the one point statistical properties of the near field of a coaxial turbulent jet are described.

##### MEAN VELOCITY MEASUREMENT

Mean velocity profiles were taken from approximately zero to eight diameters downstream. These profiles are presented in Figure 4(a). In this figure the excess local mean velocity,  $U - U_{FS}$ , is normalized by the excess centerline velocity,  $U_{max} - U_{FS}$ , and is plotted against the non-dimensional radius,  $(r - r_m)/b(x)$ . The term  $r_m$  defines the location where the velocity is the arithmetic average of its centerline and free stream value, and  $b(x)$  is the radial distance between the locations of  $\bar{U} = .20 U_{max}$  and  $\bar{U} = .80 U_{max}$ . The  $.20 U_{max}$  and  $.80 U_{max}$  were chosen because they could be determined reliably.

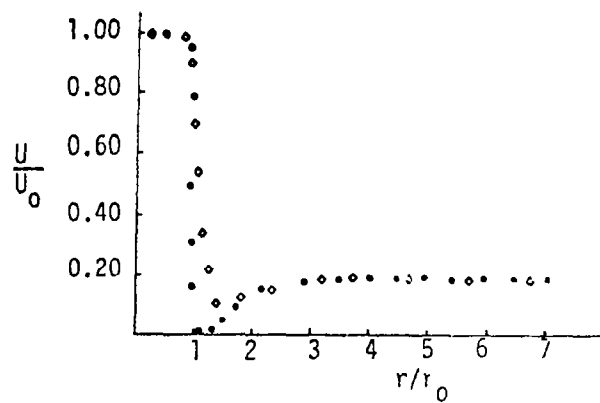


Figure 3 Pitot Static Tube Surveys of Mean Velocity

- $x/D = 0$
- ◇  $x/D = 1$

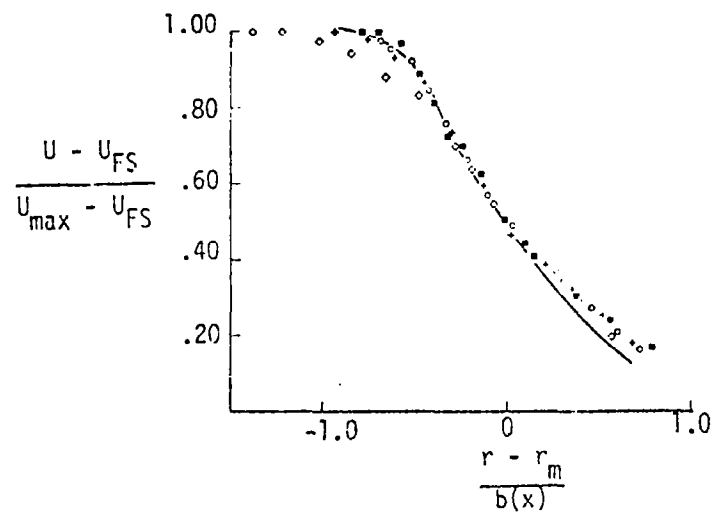


Figure 4(a) Similarity Plots of Mean Velocity Profiles

- ◇  $x/D = 2$  Author
- +  $x/D = 4$  Author
- $x/D = 6$  Author
- $x/D = 8$  Author
- Forstall, Shapiro ( $\lambda_j = 5$ )

Also in Figure 4(a), comparison of the data from this investigation and that of Forstall and Shapiro<sup>(7)</sup> is made. The data presented by Forstall and Shapiro is for a coaxial jet with  $\lambda_j = 5$ . A slight variance in the profiles is present in the region  $\frac{r - r_m}{b(x)} > 0$  where Forstall and Shapiro's coaxial jet's mean velocity decays a bit more rapidly than is true in the present investigation.

The spreading of the jet is considered in Figure 4(b). In this plot, the non-dimensionalized half-width,  $r_m/r_o$ , versus non-dimensionalized axial downstream distance,  $x/D$ , is presented. The agreement between the results of this investigation and the experimental findings of Forstall and Shapiro and also with the theoretically predicted curve by Squire and Trouncer<sup>(22)</sup> for a co-flowing jet is quite good. Corrsin's data is for a free jet. Initially the co-flowing jet spreads faster than the free jet but after 6 diameters, the trend is reversed.

#### TURBULENCE INTENSITIES

Instantaneously, the velocity at a point in a turbulent flow varies or fluctuates around a mean value. The turbulent intensity is the ratio of the root mean square of these instantaneous fluctuations to the average or mean flow.

The axial and radial distributions of the turbulence intensity

$\frac{(u^2)^{1/2}}{u_o}$  in terms of core velocity are shown in Figure 5. These values of the turbulent intensities have been corrected for ambiguity noise. The method used for determining the contribution to the turbulence level of the finite transit times of the particles in the control volume is that developed by Morton<sup>(23)</sup>. Ambiguity noise is similar to the Doppler ambiguity in the radar technique. It arises because of the finite beam width of the illuminating laser beam, or the finite transit times of the smoke particles crossing the beam. For this particular optical arrangement, the ambiguity noise was of the order of 1.7% of the mean velocity.

The turbulent intensities measured are compared to those measured by Ko and Davies<sup>(24)</sup>, Bradshaw et al.<sup>(25)</sup>, and Sami<sup>(5)</sup>.



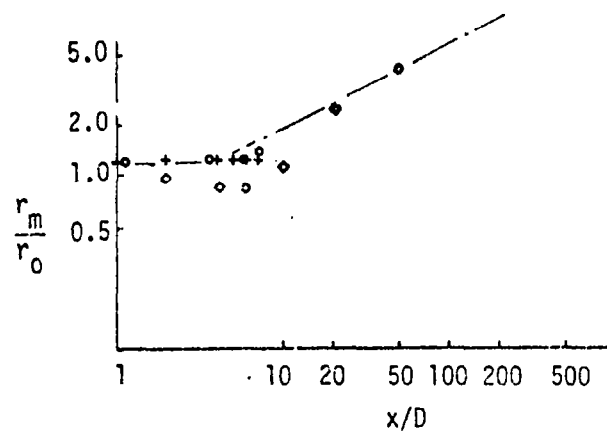


Figure 4(b) Half Boundaries of Mixing Region

+	Author	$\lambda_j = 5.1$
◇	Corrsin & Uberoi	$\lambda_j = \infty$
○	Forstall & Shapiro	$\lambda_j = 5$
----	Squire & Trouncer	

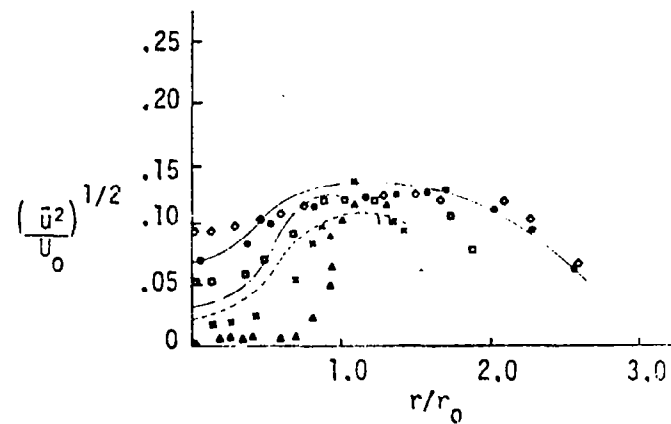


Figure 5 Turbulent Intensity Profiles at  
Five Downstream Locations

$x/D = 0$  ▲ Author  
 $x/D = 2$  × Author  
 $x/D = 4$  □ Author  
 $x/D = 6$  ● Author  
 $x/D = 8$  ◇ Author

----- Bradshaw, et al.  
 - · - · - Davies  
 \_\_\_\_\_ Sami

An important point is discerned from a comparison of the turbulent intensity and mean velocity profiles. Out to approximately 5 diameters downstream from the exit plane, the maximum intensity occurs near the radial location of the point of inflection of the mean velocity profile. This occurs at approximately 1 radius from the centerline of the jet. For distances greater than 5 diameters downstream from the nozzle exit plane, the location of the maximum value of the turbulent intensity moves out radially as the mean velocity profile tends towards a similarity form. Similarity means that profiles at any downstream location in the far field of the turbulent jet collapse onto each other when properly non-dimensionalized.

#### INTERMITTENCY

Intermittency is customarily defined as the probability that the flow is turbulent at a particular location in the flow field. In this investigation, a marked turbulent smoke jet exhausts into a low turbulence level secondary flow. The Schmidt number, which is defined as the ratio of the kinematic viscosity of air to the coefficient of diffusivity of DOP droplets has a value of approximately  $4 \times 10^4$  for this experiment. Thus, in the outer region of the jet, the presence of smoke particles implies that vorticity exists and that the flow is turbulent. Van Atta<sup>(26)</sup> has stated that discrimination with respect to a passive scalar may prove to be operationally superior to using velocity or vorticity for defining the position of the superlayer. The intermittency profiles presented in Figure 6 are compared to results of Sami<sup>(5)</sup>.

The increase in the Intermittency in the region  $r/r_0 = 1$  to  $r/r_0 = 1.5$  in Figure 6 indicates the presence of a vortex ring at the exit of the jet. This is in accordance with Davies<sup>(1)</sup>.

#### LONGITUDINAL CORRELATIONS

Autocorrelations of the axial velocity fluctuations are taken at the centerline of the jet and at a distance of 1 radius from the center of the jet for two downstream locations. The autocorrelation coefficient,  $R$ , is shown as a function of delay time in Figures 7(a)-(b).

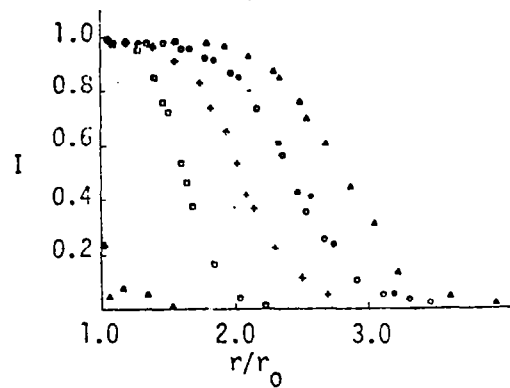


Figure 6 Intermittency Profiles at Five Downstream Locations

$x/D = 0$  Author ▲  
 $x/D = 2$  Author □  
 $x/D = 4$  Author +  
 $x/D = 6$  Author ○ Sami ●  
 $x/D = 8$  Author △

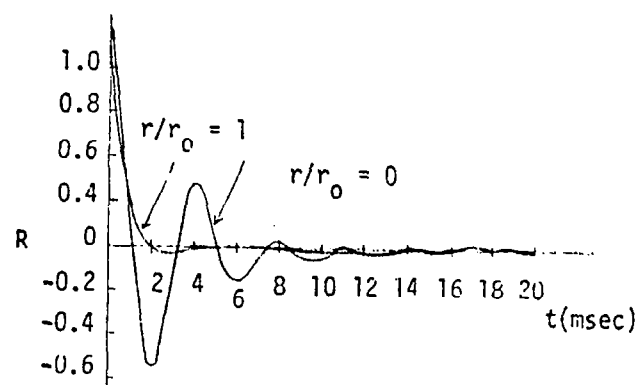


Figure 7(a) Longitudinal Autocorrelations  
 $x/D = 4$

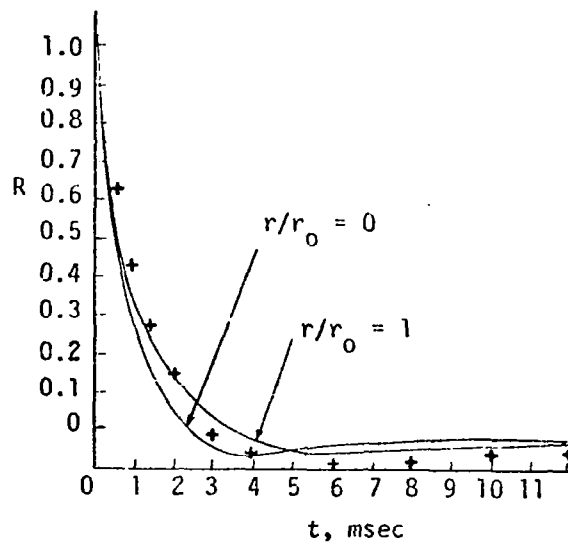


Figure 7(b) Longitudinal Autocorrelations at  $x/D = 8$

— Author  
 + Laurence ( $r/r_0 = 1.028$ )

There is a slight variance in the correlations taken by the author as compared to Laurence's<sup>(27)</sup> data. This difference, which will show up much more clearly in the spectral density plots, is probably a Reynolds number effect.

Taylor's hypothesis<sup>(28)</sup> is used to convert autocorrelations to longitudinal correlations from which two other quantities, the Taylor microscale and the integral scale, are calculated. The Taylor microscale, which is an estimate of the length scale associated with dissipation in a flow, is obtained from the curvature of the longitudinal correlation curve at zero separation.

The integral scale gives an estimate of the largest scale in the flow. It is obtained by numerically integrating the area under the longitudinal correlation curve and multiplying the result by the local mean velocity.

The values of the Taylor microscales and integral scales are tabulated as follows:

Table 2

Integral Scales,  $L$ , and Taylor Microscales,  $\lambda_T$ ,  
At several Axial Positions for  $r/r_o = 0$  and  $r/r_o = 1$

X/D	$L_{r/r_o = 0}$	$L_{r/r_o = 1}$	$\lambda_{T_{r/r_o = 0}}$	$\lambda_{T_{r/r_o = 1}}$
0	$3.435 \times 10^{-3} \text{m}$	-----	$3.517 \times 10^{-5} \text{m}$	-----
2	$5.283 \times 10^{-3} \text{m}$	$1.675 \times 10^{-3} \text{m}$	$1.728 \times 10^{-3} \text{m}$	$6.023 \times 10^{-4} \text{m}$
4	$6.095 \times 10^{-3} \text{m}$	$3.719 \times 10^{-3} \text{m}$	$1.8217 \times 10^{-3} \text{m}$	$8.563 \times 10^{-4} \text{m}$
6	$6.102 \times 10^{-3} \text{m}$	$5.112 \times 10^{-3} \text{m}$	$1.883 \times 10^{-3} \text{m}$	$9.346 \times 10^{-4} \text{m}$
8	$6.944 \times 10^{-3} \text{m}$	$6.735 \times 10^{-3} \text{m}$	$1.867 \times 10^{-3} \text{m}$	$12.096 \times 10^{-4} \text{m}$

To analyze these results, look at the values for the Taylor microscale at the centerline of the jet as compared to one radius from this location ( $r/r_o = 1$ ). For distances greater than or equal to two

diameters downstream, the Taylor microscale on the centerline remain fairly constant and somewhat larger than  $\lambda_T$  determined at  $r/r_o = 1$ . This non-dependence of  $\lambda_T$  on the downstream position is what would be expected in view of the small shears in the region.

At  $r/r_o = 1$ ,  $\lambda_T$  does grow with distance downstream. This is not unexpected in view of the fact that  $r/r_o = 1$  is in the mixing region which is growing. Another important point is to note that the value of  $\lambda_T$  close to the exit plane of the jet is two orders of magnitude smaller than the other values for  $\lambda_T$  at the centerline. At this point the turbulence level is so low that ambiguity noise predominates. Thus this  $\lambda_T$  is characteristic of noise rather than turbulence. <sup>(23)</sup>

Focusing attention next on the growth of the integral scale at the radial distance of 1 radius from the centerline of the jet, Laurence <sup>(24)</sup> predicts that the integral scale will increase linearly with downstream distance which is in agreement with Table 2.

#### SPECTRA OF TURBULENCE

In order to determine the spectral density curves, a computer program is used which takes the Fourier Transform of the autocorrelation functions. The energy spectral density curves for different downstream locations at the centerline and 1 radius out from the centerline are presented in Figure 8. The profiles are normalized so that the area underneath each curve is equal to 1. By examining the spectral density curves for different distances downstream from the nozzle exit plane, the change in the turbulence spectra is primarily a shift of energy from higher to lower frequencies with increasing  $x/D$  Ratio.

In the spectral density plots, the variance of the author's results as compared to Laurence's data once again suggests that the order of magnitude difference in the Reynolds numbers for the two flows affected the distribution of turbulent energy. With increasing Reynolds number for the same control volume location in the flow, there was observed a shift of energy to higher frequencies.



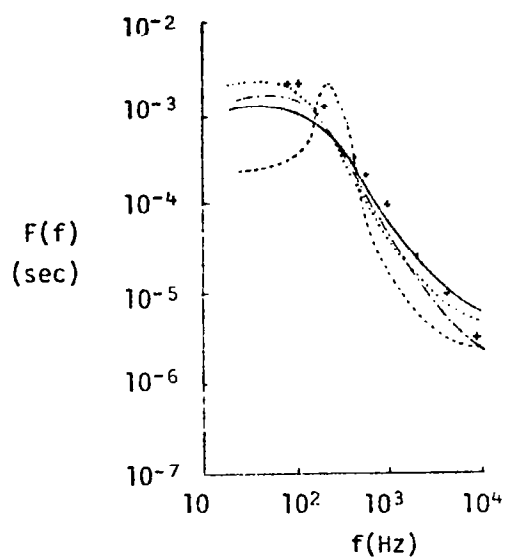


Figure 8 Spectral Density Curves at  $x/D = 4, 8$

.....	$r/r_0 = 1$	$x/D = 8$	Author
----	$r/r_0 = 0$	$x/D = 3$	Author
—	$r/r_0 = 1$	$x/D = 4$	Author
-.-.-	$r/r_0 = 0$	$x/D = 4$	Author
+	$r/r_0 = 1.028$	$x/D = 3$	Laurence

The appearance of peaks in the spectra at  $x/D = 4$  and  $r/r = 0$  is in agreement with Ko and Davies,<sup>(24)</sup> and Bradshaw et al.<sup>(25)</sup>. The spectrum shape is completely different in the potential core in comparison to that found in the mixing region. This may suggest, as has been theorized that in the core, most of the increase in energy is due to the increase in the pressure field at the dominant frequencies and very little is due to an increase in the local turbulence level. The bandwidth of the "bump" broadens as the axial distance increases. This can be explained by the propagation of the pressure field downstream<sup>(29)</sup>.

The spectral density curves outside the potential core, but in the mixing region, do not have a "bump" in the energy spectrum. The reason for this is that the high background turbulence level completely obscures the relatively small pressure fluctuations. Again, according to Davies, and also Bradshaw, this indicates that the flat part of the spectrum is due to local turbulence, while the peak represents mostly the pressure field. The Strouhal numbers corresponding to the peaks in the spectra are compared to those found by Davies in Table 3.

Table 3

$$S_{tr} = \frac{f D}{U_o}$$

<u>X/D</u>	<u>Davies</u>	<u>Author</u>
2	.530	.550
4	.498	.512
6	.420	.398
8	----	.165

### CONCENTRATION-VELOCITY-CORRELATION

The concentration-velocity correlation was also measured in this investigation. No data is available to be used as a comparison. The concentration-velocity correlation coefficient is defined as the following:

$$R_{u\theta} = \frac{\overline{u\theta}}{(\overline{u^2})^{1/2} (\overline{\theta^2})^{1/2}}$$

where  $u$  is the fluctuating velocity and  $\theta$  is the fluctuating part of the concentration, both measured at the same point and time in the flow. Three profiles are taken, one at  $x/D = 2$ , and the others at  $x/D = 4$ , and  $x/D = 8$ . These graphs are presented in Figure 9.

The significance of the concentration-velocity correlation is that it indicates how closely related the passive admixture field is with the velocity field. A zero correlation would indicate that the fluctuations in the concentration field are totally independent of the turbulent velocity fluctuations. This is the case for the profile taken at  $x/D = 2$ ,  $|r/r_0| \leq 0.2$ . Though both  $\overline{u^2}$  and  $\overline{\theta^2}$  are small in the potential core, they are not negligible. The existence of  $\overline{\theta^2}$  at the exit plane is probably due to imperfect seeding. Out from the centerline of the jet,  $R_{u\theta}$  initially becomes negative and then changes sign. It reaches a maximum value at  $r/r_0$  equal to approximately one. Vortices which would entrain "clean" air from outside the jet and accelerate the entrained fluid particles would give rise to regions of negative concentration-velocity correlation. As the potential core breaks up further downstream, the concentration and velocity fluctuations become more highly dependent.

### CONCENTRATION FIELD SPECTRA

A spectrum of concentration or contaminant fluctuations is produced when smoke particles are mixed by turbulent flow field of the jet. Many of the same concepts that are used in describing the kinetic energy

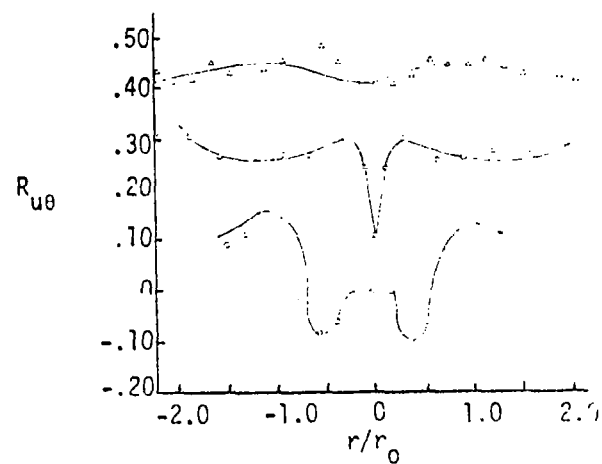


Figure 9 Concentration-Velocity Correlations

- $x/D = 2$
- $x/D = 4$
- △  $x/D = 8$

spectrum can be applied to the spectra of the mixing smoke particles. The scales of the smoke particles fluctuations range from the scale of the energy-containing eddies to a smallest scale that is dependent on the ratio of the diffusivities (Schmidt number). (28)

The spectral density curves for two different values of the  $x/D$  ratio are presented in Figure 10. These curves are taken at the radial position in the flow field where the intermittency has a value of approximately 50% (for  $x/D = 2$ ,  $r/r_o = 1.02$ ; for  $x/D = 5$ ,  $r/r_o = 2.36$ ). Note the dramatic shift of energy from the higher to the lower frequencies as the flow travels downstream.

#### MEAN RADIAL VELOCITY MEASUREMENT

Mean radial velocity profiles were taken at three downstream locations. These profiles are presented in Figure 11. In this figure, the local mean radial velocity in terms of the excess centerline velocity,

$$\frac{\bar{v}}{U_{\max} - U_{FS}},$$

, is plotted against the non-dimensional radius,  $(r - r_m)/b(x)$ .

Measurement of the mean radial velocity was much more difficult than determining the longitudinal component. This caused the scatter for the radial velocity profiles to be more pronounced than had been the case for the  $\bar{U}$  velocity component surveys. The  $\bar{v}$  velocity component was found to be almost two orders of magnitude smaller than the  $\bar{U}$  component. The  $\bar{v}$  found here are somewhat higher than that observed by Sami et al. (4) This is consistent with the fact that the initial spread of the jet is faster in the coflowing case (c.f., Figure 4(b)) and the fact that  $\bar{v}$  is "conditionally" averaged. Antonia, Prabhu, and Stephenson (30) also reported significantly higher radial mean velocities when conditionally averaged.

#### RADIAL TURBULENT INTENSITIES

The radial distributions of the turbulent intensity,  $\frac{(\overline{v^2})^{1/2}}{U}$ , in terms of the core velocity, for three downstream locations are shown in Figure 12. Once again, the radial turbulent intensities have been corrected for ambiguity noise.

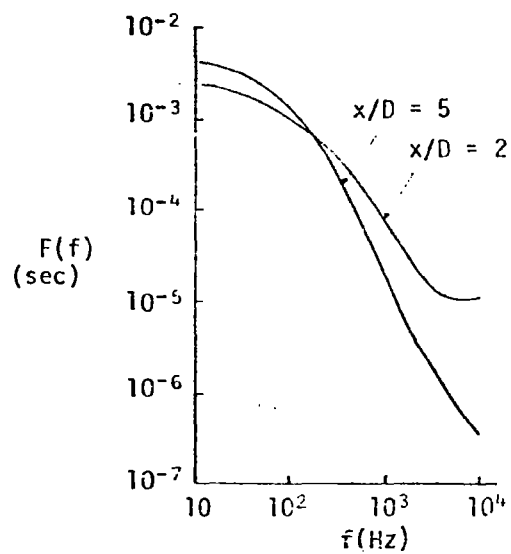


Figure 10 Concentration Spectral Density Curves

$x/D = 2$   $I = .49$

$x/D = 5$   $I = .49$

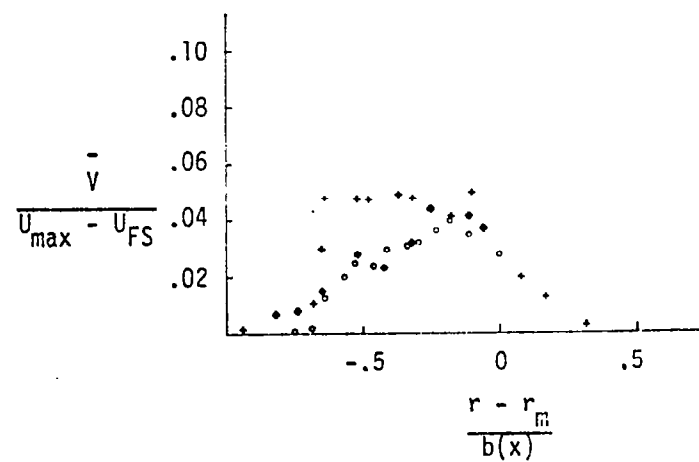


Figure 11 Mean Radial Velocity Profiles

+  $x/D = 4$

o  $x/D = 6$

◆  $x/D = 8$

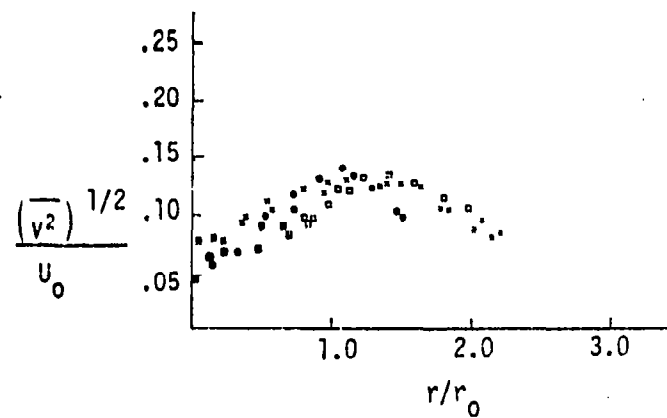


Figure 12 Radial Turbulent Intensity Profiles

●  $x/D = 4$

□  $x/D = 6$

X  $x/D = 8$



The radial turbulent intensities are of the same order of magnitude as  $\frac{\overline{(u^2)}^{1/2}}{U_0}$ , and the profiles for each downstream location are quite similar in shape to the longitudinal intensity plots.

## SUMMARY

An experimental investigation of the near field of a coaxial turbulent jet was made. Mean velocities, turbulent intensities, intermittencies, velocity autocorrelations and spectral density curves, and velocity-concentration correlation coefficients were determined. The following results were obtained:

1. When non-dimensionalized using the half velocity width and the width of the mixing region, the axial and radial mean velocity profiles collapsed adequately. There was, however, considerably more scatter in the radial mean velocity profiles.
2. For downstream locations less than  $x/D = 5$ , the maximum turbulent intensity occurs near the radial location of the point of inflection of the mean velocity profile. This occurs at approximately  $r/r_0 = 1.0$ . For a larger  $x/D$ , the location of the maximum value of the turbulent intensity moves out radially as the mean velocity profiles tend towards a similar form.
3. The Taylor microscales for the near field of the turbulent jet were determined. At the radial position  $r/r_0 = 0$ , the Taylor microscale remained constant from 2 to 8 diameters downstream from the exit plane.
4. The integral scales of the turbulent jet flow were determined. For  $r/r_0 = 1.0$ , the integral scale grew linearly, as had been predicted.
5. The energy spectral density curves had completely different shapes in the potential core as contrasted to the mixing region. In the potential core, the energy spectrum had a peak which was due to the increase in the pressure field at the dominant frequencies. In the mixing region, this "bump" could not be found because it was completely obscured by the high turbulence level.
6. The concentration-velocity correlation was determined for the first time in the near field of a turbulent jet. In the potential core region, this correlation coefficient was found to be zero.

# REFERENCES

1. Davies, P.O.A.L., "Turbulence Structure in Free Shear Layers," AIAA Journal, Vol. 4, No. 11, 1966.
2. Townsend, A. A., "The Structure of Turbulent Shear Flow," Cambridge University Press, London, 1956.
3. Lau, J. C. and M. J. Fisher, "The Vortex-Street Structure of Turbulent Jets. Part 1." Journal of Fluid Mechanics, Vol. 67, Part 11, 1975.
4. Sami, S., T. Carmody, and H. Rouse, J. Fluid Mechanics, Vol. 50, Part 2, 1967.
5. Sami, S., "Balance of Turbulence Energy in Region of Jet Flow Establishment," J. Fluid Mechanics, Vol. 29, Part 1, 1967.
6. Kuethe, A. M., "Investigation of the Turbulent Mixing Regions Formed by Jets," Journal of Applied Mechanics, Trans ASME, Vol. 57, 1935.
7. Forstall, W., Jr. and A. H. Shapiro, "Momentum and Mass Transfer in Coaxial Gas Jets," Journal of Applied Mechanics, Dec. 1950.
8. Alpinieri, L. J., "Turbulent Mixing of Coaxial Jets," AIAA Journal, Vol. 2, No. 9.
9. Wygnanski, I. and H. E. Fielder, "The Two Dimensional Mixing Region," Journal of Fluid Mechanics, Vol. 41, Part 11, 1970.
10. Antonia, R. A. and R. W. Bilger, "An Experimental Investigation of an Axisymmetric Jet in a Coflowing Air Stream," Journal of Fluid Mechanics, Vol. 61, Part IV, 1973.
11. Corrsin, S., NACA ARC No. 3123, 1943.
12. Corrsin, S. and M. S. Uberoi, NACA TN No. 1865, 1949.
13. Corrsin, S. and M. S. Uberoi, NACA Report 998, 1950.
14. Szablewski, W., "The Diffusion of a Hot Air Jet in Motion," NACA TM 1288, 1950.
15. Yeh, Y. and H. Z. Cummins, Applied Physics Letter 4, 176, 1964.
16. Cummins, H. Z., N. Knäble, and Y. Yeh, Phys. Rev. Letters 12, 150, 1964.
17. Foreman, J. W., Jr., R. D. Lewis, J. R. Thorton, and H. J. Watson, Proc. IEEE 54, 424, 1966

18. Yeh, Y. and H. Z. Cummins, Appl. Phys. Letters 4, 176, 1964.
19. Rosenweig, R. E., "Measurement and Characterization of Turbulent Mixing," Sc. D. Thesis, Massachusetts Institute of Technology, 1959.
20. Shaughnessy, E. J., Jr., "Measurement of Particle Diffusion in a Turbulent Jet by Laser Light-Scattering," Ph.D. Thesis, The University of Virginia, 1975.
21. Clark, W. H., "Measurement of Two Point Velocity Correlations in a Pipe Flow Using Laser Anemometers,": Ph.D. Thesis, The University of Virginia, 1970.
22. Squire, H. B. and J. Truncer, "Round Jets in a General Stream," ARC Technical Report R & M No. 1974, 1944.
23. Morton, J. B., "Experimental Measurement of Ambiguity Noise in a Laser Anemometer, Journal of Physics, E., Vol. 6, 1974.
24. Ko, N. W. M., and P. O. A. L. Davies, "The Near Field Within the Potential Cone of Subsonic Cold Jets, Journal Fluid Mechanics, Vol. 27, Part 1, 1971.
25. Bradshaw, P., D. H. Fevis and R. J. Johnson, "Turbulence in Noise Producing Region of Circular Jets," Journal Fluid Mechanics, Vol. 19, 1964.
26. van Atta, C. W., "Sampling Techniques in Turbulence Measurements," Annual Review of Fluid Mechanics, Vol. 6, 1974.
27. Laurence, J. C., NACA Report 1292, 1955.
28. Tennekes, H. and J. L. Lumley, "A First Course in Turbulence, The MIT Press, 1972.
29. Davies, P. O. A. L., M. J. Fisher and M. J. Banatt, "The Characteristics of the Turbulence in the Mixing Region of the Round Jet," Journal Fluid Mechanics, Vol. 15, 1963.
30. Antonia, R. A., A. Prabhu

**END**

**DATE**

**FILMED**

**AUG 19 1976**